



Study of p-n $\text{CaFe}_2\text{O}_4/\text{LaAlO}_3$ Heterojunctions for Hydrogen Production by Photocatalytic Water Splitting Process under Visible Light

H.Medjadji¹, A.Boulaouache^{1,2}, N.SALHI^{1,2,*}, M.Trari³

¹Laboratoire de Chimie Physical Molecular and Macromolecular.

(LCPMM), Faculté des Sciences, Université BLIDA1, B.P 270, Route de Soumaa, BLIDA, Algérie

²Laboratoire de Chimie du Gaz Naturel, Faculté de Chimie, USTHB, BP32, El-Alia, 16111 Bab Ezzouar, Alger, Algérie

³ Laboratoire de Stockage et valorization de l'énergie renouvelable, Faculté de Chimie, USTHB, BP32, El-Alia, 16111 Bab Ezzouar, Alger, Algérie
*n.salhi@yahoo.fr, Salhi_nassima@univ-blida.dz

Abstract: The construction of heterojunctions is widely regarded as one of the most effective strategies for suppressing charge recombination, extending the light absorption range of a single photocatalyst, and significantly enhancing hydrogen production through photocatalytic water splitting. Herein, we explore a novel heterojunction system designed to optimize charge separation and improve overall photocatalytic efficiency. The 25% CaFe_2O_4 -75% LaAlO_3 heterojunction was synthesized by mechanically mixing CaFe_2O_4 and LaAlO_3 , prepared via nitrate and sol-gel methods. Characterization techniques such as TGA-DT, XRD, XPS, UV-Vis spectroscopy, SEM-EDX, and electrochemical tests confirmed the formation of pure phases with crystallite sizes of 31 nm (CaFe_2O_4) and 36 nm (LaAlO_3). XPS analysis identified surface elements including La^{3+} , Al^{3+} , Fe^{3+} , Ca^{2+} , and O^{2-} , while SEM revealed irregular nanoparticles with moderate porosity. The photocatalyst was tested in water-splitting for hydrogen production under visible light exposure. The heterojunction significantly improved photocatalytic hydrogen production, generating 209.72 $\mu\text{mol H}_2$ in NaOH (pH ~12) under visible light, 1.62 times more than pure CaFe_2O_4 . Adding $\text{S}_2\text{O}_3^{2-}$ hole scavenger further increased H_2 production to 297.87 μmol over four cycles by reducing electron-hole recombination.

Keywords: Hydrogen production; LaAlO_3 perovskite; CaFe_2O_4 spinel; Heterojunction; Water reduction.

1. Introduction

The growing reliance on fossil fuels for energy production has significantly increased greenhouse gas emissions, driving global warming. As a result, finding sustainable and eco-friendly energy sources is essential to meet the rising energy demand. Green hydrogen offers a promising alternative, providing a cleaner and more sustainable option with a higher energy density compared to conventional sources [1-2]. However, the primary challenge is improving hydrogen production efficiency by developing materials that effectively harness visible light. One promising strategy is the formation of heterojunctions, which reduce electron-hole recombination without altering the energy levels of the original materials. P-n heterojunction systems have attracted considerable attention for their ability to generate an electric field that reduces

electron-hole recombination, thereby enhancing hydrogen production efficiency [3,4]. In this study, 25%CaFe₂O₄-75%LaAlO₃ heterojunction system was prepared using mechanical mixing method, with CaFe₂O₄ and LaAlO₃ synthesized separately via the nitrate and sol-gel routes, respectively. The study focused on assessing the heterojunction's impact on hydrogen production under visible light, with the aim of minimizing electron-hole recombination during photocatalysis. Hydrogen generation was measured under visible light to evaluate the efficiency of the heterojunction.

2. Materials and methods

LaAlO₃ was synthesized using sol-gel method. High-purity precursor salts of La(NO₃)₃·6H₂O (99%) and Al(NO₃)₃·9H₂O (98.5%), were dissolved in distilled water, with propionic acid (C₆H₇O₆) as a chelating agent. The solution was evaporated at 200°C, forming a gel, which was dried and calcined at 800°C (2°C/min) for 4 hours. CaFe₂O₄ was prepared via nitrate method by dissolving Ca(NO₃)₂·4H₂O and Fe(NO₃)₃·9H₂O in water, evaporated at 200°C, ground, and calcined at 850°C. The Heterogeneous 25%CaFe₂O₄-75%LaAlO₃ nanocomposite was synthesized through a straightforward mechanical mixing process, blending spinel CaFe₂O₄ and perovskite LaAlO₃ in an agate mortar for 30 minutes in varying proportions.

3. Characterization techniques

The crystalline phases of the powders were analyzed by X-ray diffraction (Rigaku) over a 2θ range of 20-80°. Scanning electron microscopy (SEM, JEOL JSM-7610F Plus) equipped with an EDS detector was used to examine the morphology and conduct elemental analysis. Diffuse reflectance spectra were obtained using a UV-visible spectrophotometer (Cary 5000), while the surface chemical composition was examined through X-ray photoelectron spectroscopy (XPS, Escalab 220 XL).

4. Photocatalytic activity

The photocatalytic test was carried out in a 200 mL Pyrex reactor at a constant temperature of 50 ± 1°C using an electrostatic bath. The catalyst was stirred at 300 rpm in 190 mL of aqueous electrolyte, with oxygen removed by purging with N₂ gas for 30 minutes. Photocatalytic activity was measured by exposing the system to three 13 W LEDs under visible light, with hydrogen (H₂) production serving as the efficiency metric.

5. Results and discussion

The TGA-DTA curves (**Fig. 1**) show a ~15% weight loss for that CaFe₂O₄ from 70 to 200°C due to water release, followed by significant loss (200-450°C) from the decomposition of Ca-Fe nitrates, with thermal stability around 600°C. LaAlO₃ also exhibits initial weight loss (74-170°C) from water release, with a subsequent ~31% loss (200-400°C) attributed to the decomposition of lanthanum and aluminum nitrates and

propionic acid. A plateau above 600°C indicates oxide formation, with DTA peaks supporting these results for both phases.

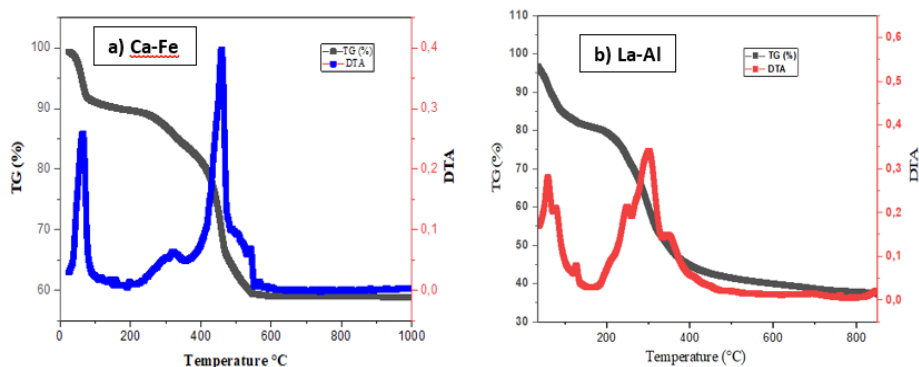


Fig.1. a,b) The thermograms of CaFe₂O₄ and LaAlO₃ before calcination

The XRD patterns of CaFe₂O₄ and LaAlO₃ are presented in **(Fig.2)**. The diffractogram of CaFe₂O₄ reveals a single-phase spinel with high crystallinity, corresponding to JCPDS Card No. 01-070-4097 and confirming cubic symmetry (space group Fd-3m). LaAlO₃ shows a pure perovskite phase, consistent with JCPDS Card No. 01-070-4104, and rhombohedral symmetry (space group R-3c). The refined lattice parameters are $a = 3.630 \text{ \AA}$ and $c = 13.103 \text{ \AA}$. Crystallite sizes, calculated using the Scherrer equation, were approximately 29 nm for CaFe₂O₄ and 36 nm for LaAlO₃.

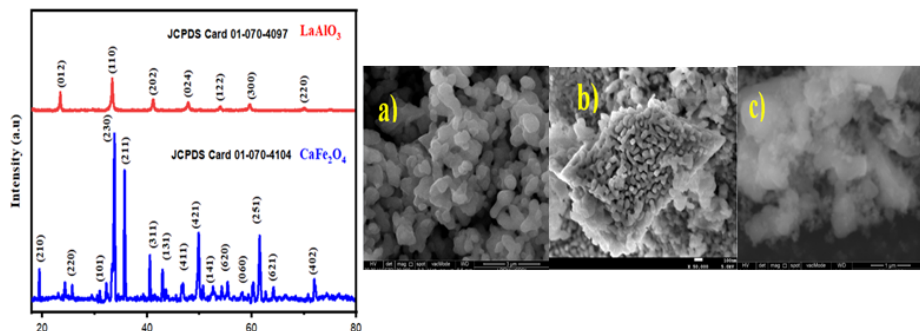
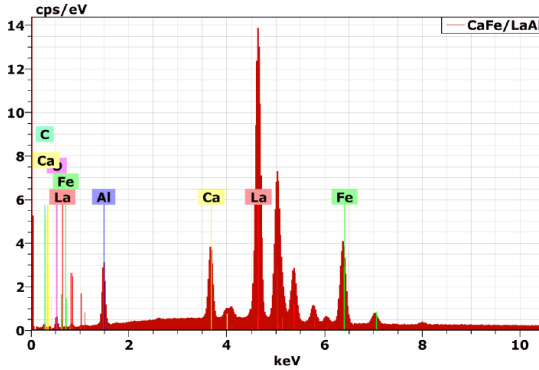


Fig.2. Diffraction patterns of CaFe₂O₄ and LaAlO₃

Fig.3. SEM images: a) CaFe₂O₄, b) LaAlO₃ and c) CaFe₂O₄ 25%/LaAlO₃

The SEM images **(Fig.3)** reveal the morphology of the raw materials and the heterojunction system. CaFe₂O₄ **(Fig.3a)** displays spherical particles with uniform grain sizes and moderate porosity, while LaAlO₃ **(Fig.3a)** shows more aggregated particles with a uniform structure. The 25%CaFe₂O₄-75%LaAlO₃ nanocomposite **(Fig.3c)** presents irregularly shaped particles. EDS analysis **(Fig. 4)** confirms the presence of Ca, Fe, La, Al, and O, validating the successful synthesis of the heterojunction

composite. The
as shown in (Fi



ing the Tauc plot,

Fig.4. EDS of 25%CaFe₂O₄-75%LaAlO₃ nanocomposite

The calculated direct band gaps for CaFe₂O₄ and LaAlO₃ were found to be 1.85 eV and 3.39 eV, respectively.

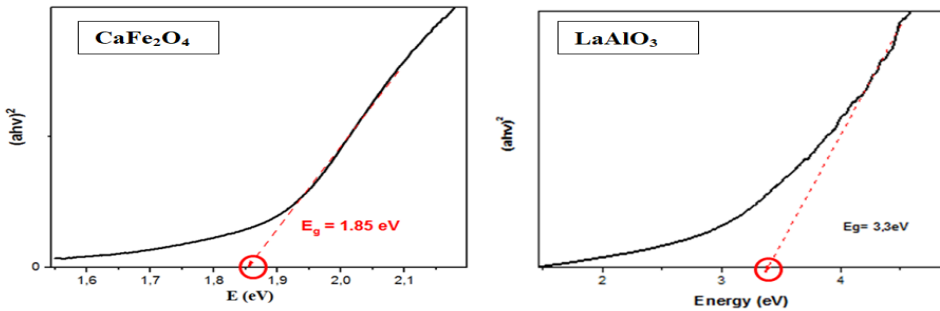


Fig.5. Tauc plots in Kubelka-Munk units for both CaFe₂O₄ and LaAlO₃ materials

XPS analysis of the 25%CaFe₂O₄-75%LaAlO₃ nanocomposite (**Fig. 6a**) confirmed the presence of Ca, Fe, La, Al, and validating the successful synthesis. The Ca 2p spectrum (**Fig.6b**) shows two distinct peaks at 345.5 eV and 355.4 eV, corresponding to Ca 2p_{3/2} and Ca 2p_{1/2}, respectively [5]. The Fe 2p spectrum (**Fig. 6c**) showed peaks in the range of 710-725 eV, corresponding to Fe 2p_{3/2} and Fe 2p_{1/2} [6,7]. The high-resolution La 3d spectrum (**Fig. 5d**) shows peaks at 848.1 eV (La 3d_{5/2}) and 866.2 eV (La 3d_{3/2}), while the Al 2p spectrum displayed a symmetric peak with a satellite at 75 eV. The O 1s spectrum (**Fig. 5f**) exhibited peaks at 529.9 eV, 531.1 eV, and 532 eV, corresponding to lattice oxygen and surface hydroxyl groups. These results align with the EDX analysis.

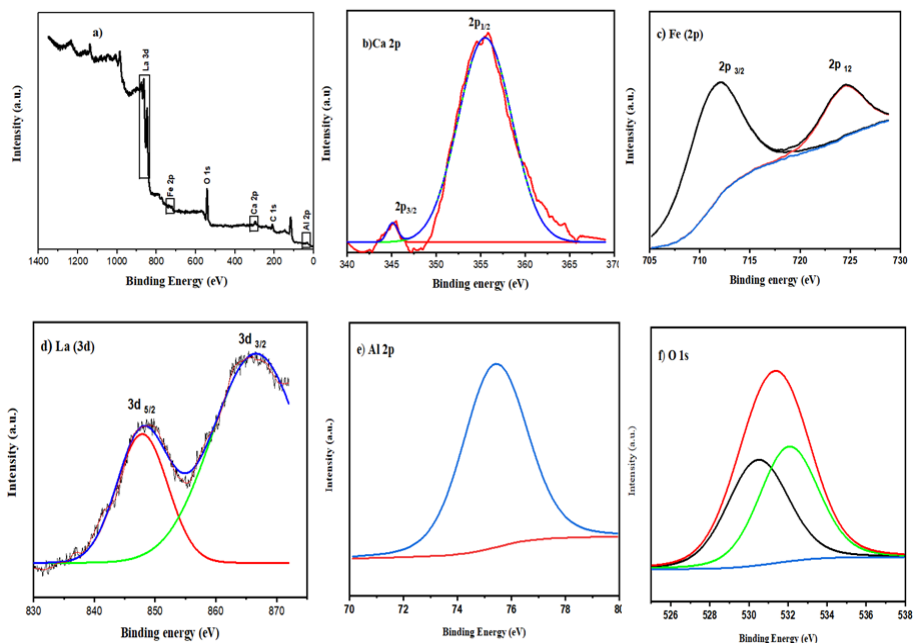


Fig.6. The XPS spectrum of 25%CaFe₂O₄-75%LaAlO₃. **a)** XPS survey, **(b, c, d, e, and f)** the binding energy of Ca, Fe, La, Al, and O

Photocatalytic activity

The hydrogen evolution during the photoreduction of water at pH ~12 is illustrated in (Fig. 7 (a)). Using CaFe₂O₄ as the photocatalyst in a 0.1 M NaOH alkaline electrolyte under visible light, around 129 μmol of hydrogen was produced in 30 minutes. In contrast, the 25%CaFe₂O₄-75%LaAlO₃ nanocomposite generated approximately 209.60 μmol of H₂ under the same conditions, yielding a 1.62-fold increase in hydrogen production compared to pure CaFe₂O₄.

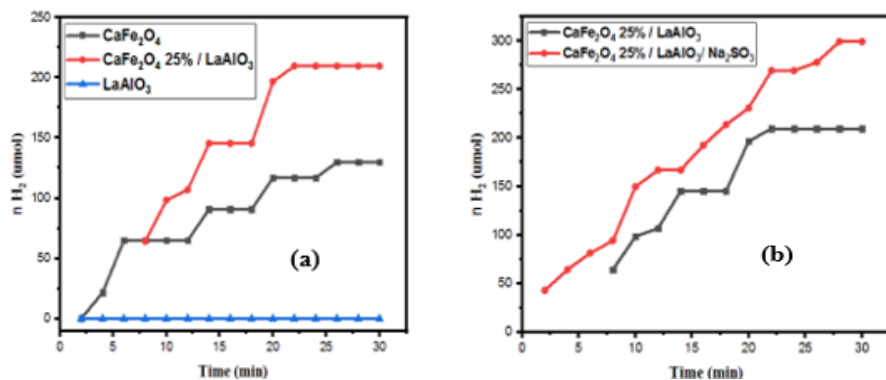


Fig.7. (a): Hydrogen evolution during the process of photo-reduction of water at pH ~12
(b):-Hydrogen evolution over 25%CaFe₂O₄-75%LaAlO₃ at pH ~12 with Na₂S₂O₃ hole sensor

This improved performance can be attributed to the heterojunction's effectiveness in reducing electron-hole recombination, enhancing charge separation and thereby increasing hydrogen generation efficiency. It is important to note that LaAlO_3 does not contribute to hydrogen production due to its wide band gap. The graph in (Fig. 7(b)) illustrates hydrogen production over time at $\text{pH} \sim 12$ (NaOH), comparing conditions with and without the hole sensor $\text{Na}_2\text{S}_2\text{O}_3$.

In presence of $\text{Na}_2\text{S}_2\text{O}_3$, hydrogen production increased by 42.11% to $297.87 \mu\text{mol}$, compared to the 25% CaFe_2O_4 -75% LaAlO_3 nanocomposite without the sensor. This improvement results from the hole-scavenging effect of $\text{Na}_2\text{S}_2\text{O}_3$, reducing electron-hole recombination. A similar enhancement was also noted in the $\text{CoFe}_2\text{O}_4/\text{LaAlO}_3$ heterojunction system [10].

The photocatalytic mechanism in the 25% CaFe_2O_4 -75% LaAlO_3 heterojunctions (Fig.8) shows an extended electron-hole pair (e^-/h^+) lifetimes. Under visible light, electrons (e^-) in CaFe_2O_4 transition from the valence band (VB) to the conduction band (CB), permitting electron transfer to LaAlO_3 's CB, reducing recombination, and thus boosting hydrogen generation through the following reaction:

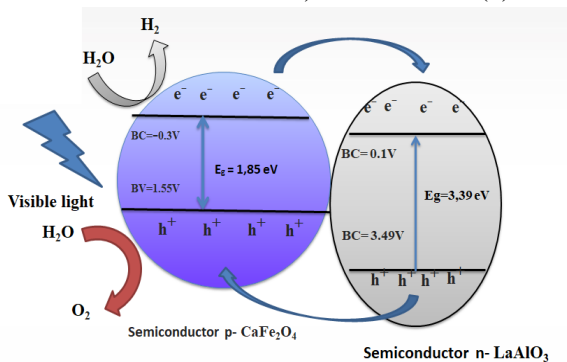
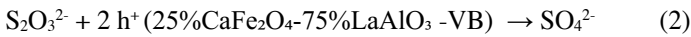


Fig.8. Photocatalytic mechanism process of water splitting for H_2 production

Conclusion

The 25% CaFe_2O_4 -75% LaAlO_3 nanocomposite was synthesized by mechanically mixing CaFe_2O_4 and LaAlO_3 . XRD analysis confirmed the presence of pure phases, with crystallite sizes of 31 nm for CaFe_2O_4 and 36 nm for LaAlO_3 . SEM images revealed irregularly shaped particles with moderate agglomeration and porosity. Photocatalytic experiments conducted for water reduction under visible light exposure showed significant enhancement in hydrogen production, with the nanocomposite yielding approximately $209.60 \mu\text{mol}$ of H_2 in a 0.1 M NaOH solution which is 1.62 times more than pure CaFe_2O_4 . The addition of the $\text{S}_2\text{O}_3^{2-}$ hole scavenger further enhanced H_2 production to $297.87 \mu\text{mol}$ over four cycles by minimizing electron-hole recombination.

References

- 1-Sebai, I., N. Salhi, G. Rekhila, and M. Trari. "Visible light induced H₂ evolution on the spinel NiAl₂O₄ prepared by nitrate route." *International Journal of hydrogen energy* 42, no. 43 (2017): 26652-26658.
- 2- Boulahouache, A., Benlembarek, M., Salhi, N., Djaballah, A.M., Rabia, C. and Trari, M., 2023. Preparation, characterization and electronic properties of LaFeO₃ perovskite as photocatalyst for hydrogen production. *International Journal of Hydrogen Energy*, 48(39), pp.14650-14658.
- 3-Shaji, Nitheesha, P. Santhoshkumar, Murugan Nanthagopal, Chenrayan Senthil, and Chang Woo Lee. "Electrochemical performance of porous CaFe₂O₄ as a promising anode material for lithium-ion batteries." *Applied Surface Science* 491 (2019): 757-764.
- 4- Han, Xiaopeng, Tianran Zhang, Jing Du, Fangyi Cheng, and Jun Chen. "Porous calcium–manganese oxide microspheres for electrocatalytic oxygen reduction with high activity." *Chemical Science* 4, no. 1 (2013): 368-376.
- 5-Shaji, Nitheesha, P. Santhoshkumar, Murugan Nanthagopal, Chenrayan Senthil, and Chang Woo Lee. "Electrochemical performance of porous CaFe₂O₄ as a promising anode material for lithium-ion batteries." *Applied Surface Science* 491 (2019): 757-764.
- 6- Benlembarek, M., N. Salhi, R. Benrabaa, A. M. Djaballah, A. Boulahouache, and M. Trari. "Synthesis, physical and electrochemical properties of the spinel CoFe₂O₄: application to the photocatalytic hydrogen production." *International Journal of Hydrogen Energy* 47, no. 15 (2022): 9239-9247.
- 7- Li, Jerry Pui Ho, Xiaohong Zhou, Yaoqi Pang, Liang Zhu, Evgeny I. Vovk, Linna Cong, Alexander P. van Bavel, Shenggang Li, and Yong Yang. "Understanding of binding energy calibration in XPS of lanthanum oxide by in situ treatment." *Physical Chemistry Chemical Physics* 21, no. 40 (2019): 22351-22358.
- 8- Potbhare, Ajay K., Prashant B. Chauke, Shadmeen Zahra, V. Sonkusare, Rina Bagade, Mayuri Ummekar, and Ratiram Gomaji Chaudhary. "Microwave-mediated fabrication of mesoporous Bi-doped CuAl₂O₄ nanocomposites for antioxidant and antibacterial performances." *Materials Today: Proceedings* 15 (2019): 454-463.
- 9-Vadivel, S., D. Maruthamani, A. Habibi-Yangjeh, Bappi Paul, Siddhartha Sankar Dhar, and Kaliyamoorthy Selvam. "Facile synthesis of novel CaFe₂O₄/g-C₃N₄ nanocomposites for degradation of methylene blue under visible-light irradiation." *Journal of colloid and interface science* 480 (2016): 126-136.
- 10-Medjadji, H., Benlembarek, M., Boulahouache, A., Derkaoui, K., Salhi, N., Trari, M. "Novel CoFe₂O₄/LaAlO₃ nanocomposites: An impressive photocatalyst with p-n hetero-junction for improved H₂ generation under visible exposure." *International Journal of hydrogen energy* 88, (2024): 878-887.

Open Access This chapter is licensed under the terms of the Creative Commons Attribution-NonCommercial 4.0 International License (<http://creativecommons.org/licenses/by-nc/4.0/>), which permits any noncommercial use, sharing, adaptation, distribution and reproduction in any medium or format, as long as you give appropriate credit to the original author(s) and the source, provide a link to the Creative Commons license and indicate if changes were made.

The images or other third party material in this chapter are included in the chapter's Creative Commons license, unless indicated otherwise in a credit line to the material. If material is not included in the chapter's Creative Commons license and your intended use is not permitted by statutory regulation or exceeds the permitted use, you will need to obtain permission directly from the copyright holder.

